Journal of Inorganic Biochemistry xxx (2015) xxx–xxx

Contents lists available at ScienceDirect

Journal of Inorganic Biochemistry

journal homepage: www.elsevier.com/locate/jinorgbio

Novel "bi-modal" H_2dedpa derivatives for radio- and fluorescence imaging

Caterina F. Ramogida [a,b], Lisa Murphy [a], Jacqueline F. Cawthray [a], James D. Ross [a], Michael J. Adam [b], Chris Orvig [a,*]

[a] Medicinal Inorganic Chemistry Group, Department of Chemistry, University of British Columbia, 2036 Main Mall, Vancouver, British Columbia V6T 1Z1, Canada
[b] TRIUMF, 4004 Wesbrook Mall, Vancouver, British Columbia V6T 2A3, Canada

ARTICLE INFO

Article history:
Received 3 September 2015
Received in revised form 12 November 2015
Accepted 17 November 2015
Available online xxxx

Keywords:
Gallium-68
Bifunctional chelates
Positron-emission tomography
Fluorescence imaging
Nitroimidazole
Spheroids

ABSTRACT

A novel pyridyl functionalized analog of the promising hexadentate $^{68}Ga^{3+}$ chelate H_2dedpa (N_4O_2, 1,2-[[6-carboxy-pyridin-2-yl]-methylamine]ethane) was successfully synthesized and characterized. This new bifunctional chelate (BFC) was used to prepare the first proof-of-principle bi-modal H_2dedpa derivative for fluorescence and nuclear imaging. Two bi-modal H_2dedpa derivatives were prepared: H_2dedpa-propyl$_{pyr}$-FITC and H_2dedpa-propyl$_{pyr}$-FITC-(*N*,*N*′-propyl-2-NI) (FITC = fluorescein, pyr = pyridyl functionalized, NI = nitroimidazole). The ligands possess the strong gallium-coordinating atoms contained within dedpa^{2-} that are ideal for radiolabeling with $^{68}Ga^{3+}$ for positron-emission tomography (PET) imaging, and two fluorophores for optical imaging. In addition, one analog contains two NI moieties for specific entrapment of the tracer in hypoxic cells. These new bi-modal analogs were compared to the native unfunctionalized H_2dedpa scaffold to determine the extent to which the addition of pyridyl functionalization would affect metal coordination, and complex stability. The non-radioactive gallium complexes were tested in a 3D tumor spheroid model. The novel pyridyl bis-functionalized H_2dedpa ligand, H_2dedpa-propyl$_{pyr}$-NH_2, was quantitatively radiolabeled with ^{67}Ga (RCY > 99%) under reaction conditions commensurate with unfunctionalized H_2dedpa (10 min at room temperature) at ligand concentrations as low as 10^{-5} M. The resultant ^{67}Ga-complex withstood transchelation to the in vivo metal-binding competitor *apo*-transferrin (2 h at 37 °C, 93% intact), signifying that [Ga(dedpa-propyl$_{pyr}$-NH_2)]$^+$ is a kinetically inert complex suitable for in vivo use, but exhibited slightly reduced stability compared to the native [^{67}Ga(dedpa)] scaffold (>99% intact). Finally, bi-model fluorescent Ga-dedpa compounds were successfully imaged in a 3D tumor spheroid model. The Ga-dedpa-FITC-NI derivative was specifically localized in the central hypoxic core of the spheroid.

1. Introduction

1.1. Molecular imaging techniques

Medical molecular imaging is defined by the ability to visualize the function of the body providing detail at the molecular and cellular level. Such techniques have become invaluable to the clinician and patient in elucidating (diagnosis) disease (especially in oncology) in early stages and providing essential information of the disease [1]. Current molecular imaging modalities available to the researcher or clinician include nuclear techniques such as single-photon emission computed tomography (SPECT) or positron emission tomography (PET), ultrasound, computed tomography (CT), magnetic resonance imaging (MRI), and optical imaging. Each modality possesses specific advantages as far as depth penetration, resolution, and image acquisition time (Table 1). Fluorescence and nuclear imaging techniques possess characteristics on opposite sides of the spectrum — resolution down to nm scale and real-time imaging can be achieved with optical imaging, whereas PET and SPECT allow for resolution only in the mm range and relatively long acquisition times are required (several minutes); the use of optical imaging is limited by its minimal penetration in tissue (mm – cm), by contrast nuclear modalities have unlimited penetration allowing whole body imaging [2,3]. The fusion of fluorescent and nuclear modalities into one imaging agent would take advantage of the strengths of each technique. For example, whole-body imaging using radio-imaging via PET to determine localization of the tumor can be supplemented by fluorescence techniques to inform clinicians (through endoscopy or surgical excision) of tumor boundaries by illuminating the cancerous cells. The synergistic blend of imaging modalities to produce bi-modal and/or multi-modal agents has been acknowledged as a promising new facet of molecular imaging with broadened applicability, and has been extensively reviewed [1–3]. Specifically, the development of bimodal radio- and fluorescent imaging probes is emerging as a potentially powerful new technique [4,5].

1.2. Radiometals in radiopharmaceuticals: Gallium-68

Metals continue to play an important role in the field of nuclear medicine. Radioactive metals possess a range of half-lives, and decay

* Corresponding author.
E-mail address: orvig@chem.ubc.ca (C. Orvig).

http://dx.doi.org/10.1016/j.jinorgbio.2015.11.021
0162-0134/

Table 1
Comparison of imaging modalities with corresponding penetration through tissue, resolution of technique, and acquisition timescale [2].

Modality	Penetration	Resolution	Timescale for acquisition/ observation
CT	Whole body	μm	Min
MRI	Whole body	μm	Min–hour
PET	Whole body	mm	Min–hour
SPECT	Whole body	mm	Min–hour
Fluorescence microscopy (optical)	mm–cm	nm	Sec
Ultrasound	Whole body except lungs	μm	Sec

emissions which make them ideal for incorporation into radiopharmaceuticals for both imaging and/or therapy.

With a half-life of 68 min and predominant positron emission (β^+, 89%), ^{68}Ga is an attractive radiometal for incorporation into a positron-emission tomography (PET) imaging agent. Moreover, the isotope can be supplied via a commercially available ^{68}Ge/^{68}Ga generator system, thus greatly enhancing the isotope's accessibility to hospitals.

Like other radiometal-based radiopharmaceuticals, the utility of ^{68}Ga-based PET imaging agents is strongly dependent on a bifunctional chelate (BFC) that possesses the ability to efficiently and securely complex the metal under radiochemical reaction conditions, such as room temperature and low concentrations. The BFC must also possess a handle for attachment to biologically relevant molecules which will act as the vehicle to enforce site-specific delivery of the pharmaceutical to the diseased state in vivo. The current state-of-the-art ligands for ^{68}Ga include the two macrocycles, 1,4,7-triazacyclononane-1,4,7-triacetic acid (NOTA) and 1,4,7,10-tetraazacyclododecane-1,4,7,10-tetraacetic acid (DOTA) [6–9]. NOTA has been universally recognized as the best chelating ligand for gallium — the binding constants are the highest reported, and complexation occurs within minutes at room temperature. Bifunctional variants of these macrocyclic (closed-chain) ligands have been prepared (e.g. NODASA and NODAGA, Fig. 1) [10–12] and conjugated to a variety of bio-targeting groups [13,14]. However, the synthesis of these ligand systems is far from trivial, and groups wishing to use these macrocycles for in vitro studies often purchase the bifunctional derivatives from commercial sources.

Our group recently reported a new acyclic (open-chain) ligand, H_2dedpa (N_4O_2, 1,2-[[6-carboxy-pyridin-2-yl]-methylamine]ethane), whose properties rival those of the gold standard NOTA for Ga(III) chelation [17,18]. This hexadentate chelating system exhibits several properties of merit for use in Ga(III) PET imaging agent elaboration: quantitative radiolabeling (radiochemical yield, RCY > 99%) in only 10 min at room temperature at ligand concentrations as low as 10^{-7} M, and metal-complexes of high thermodynamic stability and kinetic inertness. A bifunctional analog (derivative with a chemically reactive/compatible attachment for coupling to biomolecules/targeting vectors) of H_2dedpa was synthesized (H_2dedpa-*p*-Bn-NCS, Fig. 1) and complexed to c(RGDyK) as a proof-of-principle [15]; however, the lengthy and challenging synthesis resulted in extremely poor yields. Therefore, a synthetic route to a novel bifunctional H_2dedpa derivative would add value to this Ga(III) ligand as a viable alternative to NOTA for PET imaging agent elaboration. Herein, a novel bifunctional H_2dedpa analog possessing two reactive primary amines (H_2dedpa-propyl$_{pyr}$-NH_2, Fig. 1; pyr = pyridyl) attached to the pyridyl rings was synthesized for the first time.

The novel bifunctional H_2dedpa analog was used to prepare two bi-modal H_2dedpa derivatives. These novel compounds possess two attached fluorophores suitable for fluorescence microscopy imaging, and retain the N_4O_2 binding sphere provided by the H_2dedpa ligand for coordination to $^{68}Ga^{3+}$ for PET imaging. The second analog contains two 2-nitroimidazole (2-NI) moieties to investigate the specific uptake of the probe in hypoxic tissue, given that 2-NI can be reduced and retained exclusively in hypoxic cells via direct competition with intracellular oxygen concentration [19–22]. We recently reported 2-NI analogs of H_2dedpa which do not possess fluorophores, and exhibited superb hypoxic-to-normoxic uptake ratios in three cell lines [23]. Much effort has been made by others to make a fluorescent probe of hypoxia [24–28].

The ability of the new H_2dedpa BFCs to label gallium isotopes was investigated, followed by assessment of their kinetic inertness via an *apo*-transferrin stability assay. Finally, the optical properties of the novel "bi-modal" probes were evaluated in a 3D tumor spheroid in vitro model visualized using confocal fluorescence microscopy.

2. Experimental

2.1. Materials and methods

All solvents and reagents were purchased from commercial suppliers (Sigma Aldrich, TCI America, Fisher Scientific) and were used as received. Fluorescein isothiocyanate (FITC) was purchased from Sigma-Aldrich and used as received. Human *apo*-transferrin was purchased from Sigma Aldrich. The analytical thin-layer chromatography (TLC) plates were aluminum-backed ultrapure silica gel 60 Å, 250 μm thickness; the flash column silica gel (standard grade, 60 Å, 40–63 μm) was provided by Silicycle. ^{1}H and ^{13}C NMR spectra were recorded at 25 °C unless otherwise noted on Bruker AV300, AV400, or AV600 instruments; NMR spectra are expressed on the δ scale and referenced to residual solvent peaks. Low-resolution mass spectrometry was performed using a Waters ZG spectrometer with an ESCI electrospray/chemical-ionization source, and high-resolution electrospray–ionization mass spectrometry (HR–ESI–MS) was performed on a Micromass LCT time-of-flight instrument at the Department of Chemistry, University of British Columbia. ^{67}Ga-(chelate) *apo*-transferrin stability experiments were analyzed using GE Healthcare Life Sciences PD-10 desalting columns (size exclusion for MW < 5000 Da) and counted with a Capintec CRC 15R well counter. The HPLC system used for analysis and purification of nonradioactive compounds consisted of a Waters 600 controller, Waters 2487 dual

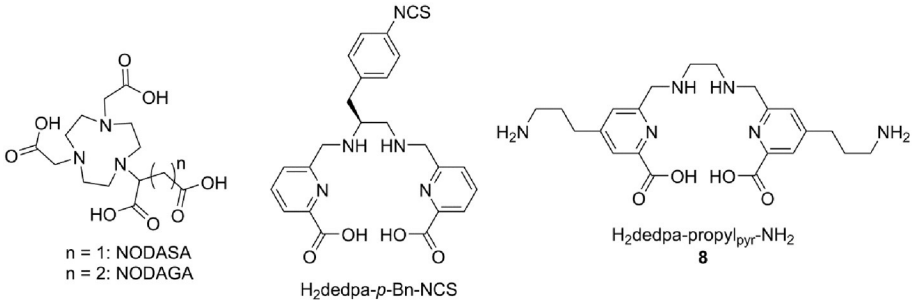

Fig. 1. Left: Bifunctional NOTA analogs used in bioconjugation reactions to targeting vectors; middle: previously synthesized bifunctional H_2dedpa derivative H_2dedpa-*p*-Bn-NCS [15,16], right: novel pyridyl bifunctional H_2dedpa derivative (**8**) synthesized in this work.

Please cite this article as: C.F. Ramogida, et al., Novel "bi-modal" H2dedpa derivatives for radio- and fluorescence imaging, J. Inorg. Biochem. (2015), http://dx.doi.org/10.1016/j.jinorgbio.2015.11.021

wavelength absorbance detector, and a Waters delta 600 pump. Phenomenex Synergi Hydro-RP 80 Å columns (250 mm × 4.6 mm analytical or 250 mm × 21.2 mm semipreparative) were used for purification of several of the deprotected ligands. Analysis of radiolabelled complexes was carried out using a Phenomenex Synergi 4 μ Hydro-RP 80 Å analytical column (250 × 4.60 mm 4 μm) using a Waters Alliance HT 2795 separation module equipped with a Raytest Gabi Star NaI (Tl) detector and a Waters 996 photodiode array (PDA). $^{67}GaCl_3$ was cyclotron-produced and provided by Nordion (Vancouver, BC, Canada) as a ~0.1 M HCl solution.

2.2. Dimethyl 4-bromopyridine-2,6-dicarboxylate (1)

Compound **1** was prepared via a slightly modified version from previously published [29]. Chelidamic acid monohydrate (2.20 g, 10.9 mmol) and PBr_5 (23.4 g, 54.3 mmol, 5 equiv) were heated neat to 90 °C under N_2 for 2 h. The deep red melt was then cooled to room temperature, and $CHCl_3$ (25 mL) was added. The solution was filtered, and filtrate was cooled on ice (0 °C), while methanol (90 mL) was slowly added. Crystallization was induced with scratching, and the crystalline solid was collected by vacuum filtration and further dried under vacuum to yield **1** as a crystalline white solid (2.82 g, 86%). ^{1}H NMR (300 MHz, $CDCl_3$) δ 8.45 (s, 2H), 4.02 (s, 6H).

2.3. Methyl 4-bromo-6-(hydroxymethyl)picolinate (2)

Compound **1** (5.61 g, 20.5 mmol) was stirred in methanol/CH_2Cl_2 (200 mL: 50 mL) on ice (0 °C), and $NaBH_4$ (1.17 g, 30,8 mmol, 1.5 equiv) was added in small portions. The reaction mixture was stirred at 0 °C for 1.5 h, until complete by TLC (R_f (product) = 0.5, R_f (starting material) = 0.63 in 100% ethyl acetate), subsequently quenched with sat. $NaHCO_3$ (100 mL), and phases separated. The aqueous phase was extracted further with CH_2Cl_2 (4 × 50 mL); all organics were collected, dried over $MgSO_4$ and concentrated in vacuo to yield the crude product **2** as a white solid (4.79 g, 95%). The product was used in the next step without purification.

2.4. Methyl 4-bromo-6-(bromomethyl)picolinate (3)

Compound **2** (4.79 g, 19.5 mmol) was suspended with stirring in $CHCl_3$ (220 mL) at 0 °C. To this solution, PBr_3 (2.94 mL, 31.1 mmol, 1.6 equiv) was added, and the mixture was stirred at room temperature for 3.5 h. The yellow solution was subsequently cooled to 0 °C, and quenched with aq. K_2CO_3 (200 mL). The organic phase was separated, and the aqueous layer was further extracted with CH_2Cl_2 (2 × 120 mL). The organics were collected, dried over $MgSO_4$ and concentrated in vacuo. The crude solid was purified by column chromatography (CombiFlash R_f automated column system; 80 g HP silica; A: hexanes, B: ethyl acetate, 100% A to 100% B gradient) to yield **3** as a white solid (4.27 g, 67%). ^{1}H NMR (400 MHz, $CDCl_3$) δ 8.21 (d, J = 1.6 Hz, 1H), 7.86 (d, J = 1.6 Hz, 1H), 4.59 (s, 2H), 4.02 (s, 3H). ^{13}C NMR (101 MHz, $CDCl_3$) δ 164.4, 158.7, 148.7, 134.8, 130.3, 128.0, 53.5, 32.2. MS (ES+) m/z = 310.1 $[M + H]^+$.

2.5. Dimethyl 6,6′-((ethane-1,2-diylbis(((2-nitrophenyl)sulfonyl) azanediyl))bis(methylene))bis(4-bromopicolinate) (4)

Compound **3** (889 mg, 2.88 mmol, 2 equiv) and *N*,*N*′-(ethane-1,2-diyl)bis(2-nitrobenzenesulfonamide) [16] (619 mg, 1.44 mmol) were dissolved in dimethylformamide (7 mL), and Na_2CO_3 (915 mg, 8.64 mmol, 6 equiv) was added. The reaction mixture was stirred at room temperature for 3 days; subsequently diethyl ether (20 mL) and water (20 mL) were added. The white precipitate that formed upon addition was collected by vacuum filtration, washed with excess water and diethyl ether, and further dried under vacuum to yield **4** as a white solid (1.13 g, 89%). ^{1}H NMR (300 MHz, $CDCl_3$) δ 8.06 (m, 4H), 7.65 (m, 8H), 4.73 (s, 4H), 3.95 (d, J = 11.8 Hz, 6H), 3.60 (s, 4H). ^{13}C NMR (101 MHz, DMSO) δ 163.6, 157.9, 147.9, 147.5, 134.7, 133.6, 132.5, 131.4, 130.0, 128.5, 126.5, 124.4, 52.8, 52.1, 47.4. HR–ESI–MS m/z for $C_{30}H_{26}^{79}Br_2N_6NaO_{12}S_2$ ($M + Na^+$) calcd. (found) 906.9315 (906.9296).

2.6. Dimethyl 6,6′-((ethane-1,2-diylbis(((2-nitrophenyl)sulfonyl) azanediyl))bis(meth-ylene))bis(4-(3-((tert-butoxycarbonyl) amino)prop-1-yn-1-yl)picolinate) (5)

Compound **4** (420 mg, 0.47 mmol) was suspended in freshly distilled THF (20 mL) and triethylamine (8 mL) in a Schlenk flask under N_2. The vessel underwent three freeze–pump–thaw cycles to eliminate any oxygen, then *tert*-butyl prop-2-yn-1-ylcarbamate (273 mg, 1.76 mmol, 3.7 equiv), bis(triphenylphospine)palladium(II) dichloride (33 mg, 0.047 mmol, 10 mol%), and copper iodide (18 mg, 0.095 mmol, 20 mol%) were all added quickly. The flask was heated to 60 °C and stirred overnight. The resultant murky brown solution was cooled to room temperature, filtered, washed with CH_2Cl_2 and concentrated in vacuo. The crude product was purified by column chromatography (CombiFlash R_f automated column system; 24 g HP silica; A: hexanes, B: ethyl acetate, 100% A to 100% B gradient) to yield **5** as a brown fluffy solid (382 mg, 78%). ^{1}H NMR (400 MHz, $CDCl_3$) δ 8.03–7.98 (m, 2H), 7.82 (s, 2H), 7.68–7.56 (m, 6H), 7.37 (s, 2H), 4.63 (s, 4H), 4.13 (d, J = 4.2 Hz, 4H), 3.87 (s, 6H), 3.49 (s, 4H), 1.42 (s, 18H). ^{13}C NMR (101 MHz, $CDCl_3$) δ 164.7, 156.6, 155.4, 147.9, 147.6, 133.9, 133.3, 132.3, 132.1, 131.2, 127.3, 126.2, 124.3, 92.9, 80.2, 79.4, 53.5, 53.1, 52.9, 47.1, 28.3. HR–ESI–MS m/z for $C_{46}H_{51}N_8O_{16}S_2$ ($M + H^+$) calcd. (found) 1035.2864 (1035.2865).

2.7. Dimethyl 6,6′-((ethane-1,2-diylbis(((2-nitrophenyl)sulfonyl) azanediyl))bis(meth-ylene))bis(4-(3-((tert-butoxycarbonyl) amino)propyl)picolinate) (6)

Compound **5** (382 mg, 0.37 mmol) was dissolved in ethyl acetate (40 mL), and palladium on activated carbon (10% Pd, 46 mg) was added. The system was sealed and charged with hydrogen gas several times. The solution was stirred under hydrogen at room temperature for 24 h, after which time the catalyst was filtered off and replaced anew, with further stirring for an additional 24 h. The solid catalyst was filtered off, and filtrate was concentrated in vacuo to obtain **6** as a brown solid (325 mg, 84%). ^{1}H NMR (400 MHz, $CDCl_3$) δ 8.22 (m, 2H), 7.81 (s, 2H), 7.60–7.70 (m, 6H), 7.39 (s, 2H), 4.73 (s, 4H), 3.94 (s, 6H), 3.50 (s, 4H), 3.14 (quart, J = 8 Hz, 4H), 2.67 (t, J = 8 Hz, 4H), 1.79 (quint, J = 8 Hz, 4H), 1.45 (s, 18H). ^{13}C NMR (101 MHz, $CDCl_3$) δ 165.3, 156.3, 156.0, 153.5, 148.1, 147.6, 133.6, 132.6, 132.0, 131.5, 126.0, 124.6, 124.0, 79.4, 53.2, 52.8, 46.4, 40.0, 32.4, 30.5, 28.4. HR–ESI–MS m/z for $C_{46}H_{59}N_8O_{16}S_2$ ($M + H^+$) calcd. (found) 1043.3490 (1043.3472).

2.8. Dimethyl 6,6′-((ethane-1,2-diylbis(azanediyl))bis(methylene)) bis(4-(3-((tert-butoxy-carbonyl)amino)propyl)picolinate) (7)

Compound **6** (324 mg, 0.31 mmol) was dissolved in THF (10 mL), and thiophenol (65 μL, 0.64 mmol, 2.05 equiv), followed by K_2CO_3 (257 mg, 1.86 mmol, 6 equiv) was added. The reaction mixture was stirred at room temperature for 4 days; subsequently the excess salts were removed by centrifugation (10 min, 4000 rpm) and the filtrate was concentrated in vacuo. The crude product was purified by column chromatography (CombiFlash R_f automated column system; 12 g HP silica; A: dichloromethane, B: methanol with 2% triethylamine, 100% A to 25% B gradient) to obtain **7** as a light yellow-brown oil (132 mg, 63%). ^{1}H NMR (400 MHz, $CDCl_3$) δ 7.83 (s, 2H), 7.43 (s, 2H), 4.01 (s, 4H), 3.96 (s, 6H), 3.15 (quart, J = 8 Hz, 4H), 2.85 (s, 4H), 2.70 (t, J = 8 Hz, 4H), 1.84 (quint, J = 8 Hz, 4H, quint), 1.43 (s, 18H). ^{13}C NMR (101 MHz, $CDCl_3$) δ 165.9, 160.2, 155.9, 152.6, 147.5, 125.7, 123.8,

Please cite this article as: C.F. Ramogida, et al., Novel "bi-modal" H2dedpa derivatives for radio- and fluorescence imaging, J. Inorg. Biochem. (2015), http://dx.doi.org/10.1016/j.jinorgbio.2015.11.021

79.3, 54.7, 52.8, 48.7, 39.9, 32.3, 30.5, 28.4. HR–ESI–MS m/z for $C_{34}H_{53}N_6O_8$ ($M + H^+$) calcd. (found) 673.3925 (673.3928).

2.9. 6,6′-((Ethane-1,2-diylbis(azanediyl))bis(methylene)) bis(4-(3-aminopropyl) picolinic acid) (8)

Compound **7** (73 mg, 0.11 mmol) was dissolved in THF/water (3:1, 4 mL), and lithium hydroxide (11 mg, 0.43 mmol, 4 equiv) was added. The reaction mixture was stirred at room temperature for 1 h, and subsequently concentrated in vacuo. The resulting solids were redissolved in 4 M HCl/dioxane/THF (3:2:1, 8 mL), and stirred at room temperature overnight. The reaction mixture was then concentrated in vacuo and purified by semi-preparative RP-HPLC (gradient: A: 0.1% TFA (trifluoroacetic acid) in water, B: CH_3CN, 5 to 100% B linear gradient over 25 min, 10 mL/min, $t_R = 8.6$ min). Product fractions were pooled, and lyophilized to yield **8** as an off-white solid (26 mg, 55%). ^{1}H NMR (400 MHz, D_2O) δ 8.03 (s, 2H), 7.57 (s, 2H), 4.62 (s, 4H), 3.69 (s, 4H), 3.01 (t, $J = 8$ Hz, 4H), 2.83 (t, $J = 8$ Hz, 4H), 2.02 (quint, $J = 8$ Hz, 4H). ^{13}C NMR (101 MHz, D_2O) δ 168.5, 154.1, 150.9, 148.0, 126.3, 125.3, 50.2, 44.0, 38.9, 31.3, 27.1. HR–ESI–MS m/z for $C_{22}H_{33}N_6O_4$ ($M + H^+$) calcd. (found) 445.2563 (445.2570).

2.10. Dimethyl 6,6′-((ethane-1,2-diylbis((3-(2-nitro-1H-imidazol-1-yl) propyl)azane-diyl))bis(methylene))bis(4-(3-((tert-butoxycarbonyl) amino)propyl)picolinate) (9)

Compound **7** (60 mg, 0.089 mmol) and 1-(3-bromopropyl)-2-nitro-1*H*-imidazole [23] (46 mg, 0.20 mmol, 2.2 equiv) were dissolved in acetonitrile (4 mL), and K_2CO_3 (49 mg, 0.36 mmol, 4 equiv) was added. The reaction mixture was stirred at 55 °C for 4 days, subsequently cooled to room temperature, filtered to remove excess salts and concentrated in vacuo. The crude product was purified by column chromatography (CombiFlash R_f automated column system; 4 g HP silica; A: dichloromethane, B: methanol, 100% A to 30% B gradient) to yield **9** as a yellow oil (30 mg, 34%). ^{1}H NMR (400 MHz, $CDCl_3$) δ 7.82 (s, 2H), 7.38 (s, 2H), 7.19 (d, $J = 9.4$ Hz, 2H), 7.07 (s, 2H), 4.42 (t, $J = 7.2$ Hz, 4H), 3.93 (s, 6H), 3.77 (s, 4H), 3.13 (dd, $J = 13.2$, 6.7 Hz, 4H), 2.71–2.66 (m, 4H), 2.63 (s, 4H), 2.54 (s, 4H), 2.02–1.92 (m, 4H), 1.81 (dt, $J = 14.6$, 7.2 Hz, 4H), 1.40 (s, 18H). ^{13}C NMR (101 MHz, $CDCl_3$) δ 165.9, 156.1, 152.8, 147.6, 144.9, 128.5, 126.6, 126.3, 124.2, 79.4, 60.3, 53.0, 51.8, 51.4, 48.4, 40.1, 32.5, 30.8, 28.5, 28.3. MS (ES+) m/z = 979.6 $[M + H]^+$.

2.11. 6,6′-((Ethane-1,2-diylbis((3-(2-nitro-1H-imidazol-1-yl)propyl) azanediyl)) bis(methylene))bis(4-(3-aminopropyl)picolinic acid) (10)

Compound **9** (30 mg, 0.03 mmol) was dissolved in THF/water (3:1, 4 mL), and lithium hydroxide (3 mg, 0.12 mmol, 4 equiv) was added. The mixture was stirred at room temperature until methyl deprotection was deemed complete by mass spectrometry (MS (ES+) m/z = 951.7 $[M + H]^+$, about 1 h), and subsequently concentrated in vacuo. The residue was redissolved in 4 M HCl/dioxane/THF (3:2:1, 3 mL) and stirred at room temperature overnight. The reaction mixture was subsequently concentrated in vacuo, redissolved in water and purified by semi-preparative RP-HPLC (gradient: A: 0.1% TFA (trifluoroacetic acid) in water, B: CH_3CN, 5 to 100% B linear gradient over 25 min, 10 mL/min, $t_R = 12.7$ min). Product fractions were pooled, and lyophilized to yield **10** as an off-white solid (23 mg, 100%). ^{1}H NMR (400 MHz, MeOD) δ 7.92 (s, 2H), 7.49 (s, 2H), 7.42 (s, 2H), 7.11 (s, 2H), 4.49–4.44 (m, 4H), 4.42 (s br, 4H), 3.58 (s br, 4H), 3.22 (s br, 4H), 3.03–2.97 (m, 4H), 2.85–2.79 (m, 4H), 2.26 (s br, 4H), 2.03 (dd, $J = 14.5$, 7.1 Hz, 4H). ^{13}C NMR (101 MHz, MeOD) δ 167.2, 154.7, 149.0, 145.9, 128.8, 128.4, 128.1, 125.8, 119.1, 116.2, 59.3, 58.2, 53.7, 51.7, 40.1, 32.6, 28.8, 27.1. HR–ESI–MS m/z for $C_{34}H_{47}N_{12}O_8$ ($M + H^+$) calcd. (found) 751.3640 (751.3635) (−0.7 PPM).

2.12. H_2dedpa-propyl$_{pyr}$-FITC (11)

To a solution of **8** (3.5 mg, 0.008 mmol) in water (0.3 mL), a solution of fluorescein isothiocyanate (FITC) (6.1 mg, 0.016 mmol, 2.1 equiv) in DMF/water (3:1, 1.2 mL) was added. To this yellow mixture, triethylamine (5.5 μL, 5 equiv) was added at which time the solution turned much brighter orange in color. The reaction mixture was stirred at ambient temperature under darkness for 18 h. The reaction mixture was subsequently concentrated in vacuo, redissolved in CH_3CN and purified by RP-HPLC (gradient: A: 0.1% TFA (trifluoroacetic acid) in water, B: CH_3CN; 5 to 100% B linear gradient over 25 min, 1 mL/min, t_R (mono-FITC) = 16.7 min, t_R (product) = 18.7 min, t_R (FITC) = 23.4 min). Product fractions were pooled and lyophilized to yield the product as a yellow solid (3.2 mg, 33%). Purity was confirmed by HPLC re-injection of an aliquot of final collected product. HR–ESI–MS m/z for $C_{64}H_{55}N_8O_{14}S_2$ ($M + H^+$) calcd. (found) 1223.3279 (1223.3286) (0.6 PPM).

2.13. H_2dedpa-propyl$_{pyr}$-FITC-(N,N′-propyl-2-NI) (12)

Compound **10** (4.0 mg, 0.005 mmol) was dissolved in DMF/water (2:1, 0.3 mL) and FITC (4.6 mg, 0.012 mmol, 2.2 equiv) in DMF (0.1 mL) was added. To this murky yellow solution, triethylamine (3 μL, 4 equiv) was added at which time the solution turned clear and became much brighter orange in color. The reaction mixture was stirred at ambient temperature excluded from light for 20 h. The reaction mixture was subsequently concentrated in vacuo, redissolved in CH_3CN and purified by RP-HPLC (gradient: A: 0.1% TFA (trifluoroacetic acid) in water, B: CH_3CN; 5 to 100% B linear gradient over 25 min, 1 mL/min, t_R (product) = 18.4 min). Product fractions were pooled and lyophilized to yield the product as a bright yellow solid (2.9 mg, 36%). Purity was confirmed by HPLC re-injection of an aliquot of final collected product. HR–ESI–MS m/z for $C_{76}H_{69}N_{14}O_{18}S_2$ ($M + H^+$) calcd. (found) 1529.4356 (1529.4352) (−0.3 PPM).

2.14. [Ga(dedpa-propyl$_{pry}$-NH$_2$)][NO$_3$], [Ga(8)][NO$_3$]

To a solution of **8** (5.6 mg, 0.013 mmol) in water/methanol (2:1, 0.5 mL), a solution of $Ga(NO_3)_3 \cdot 6H_2O$ (5.0 mg, 0.014 mmol, 1.1 equiv) in water (0.2 mL) was added. The pH of this solution was adjusted to 5 using aq. NaOH (0.1 M), and subsequently stirred at 60 °C for 40 min. The solvent was then removed in vacuo to yield [Ga(**8**)][NO_3] as a white solid. The product was used in subsequent steps without further purification. ^{1}H NMR (400 MHz, D_2O) δ 8.28 (s, 2H), 8.00 (s, 2H), 4.70 (d, $J = 17.8$ Hz, 2H), 4.42 (d, $J = 17.8$ Hz, 2H), 3.32 (d, $J = 9.9$ Hz, 2H), 3.12 (dd, $J = 14.5$, 6.8 Hz, 8H), 2.67 (d, $J = 10.0$ Hz, 2H), 2.24–2.09 (m, 4H). ^{13}C NMR (150 MHz, D_2O) δ 167.5, 164.0, 152.8, 144.9, 129.3, 125.9, 50.9, 48.6, 40.7, 34.1, 28.8. HR–ESI–MS m/z for $C_{22}H_{30}^{69}GaN_6O_4$ (M^+) calcd. (found) 511.1584 (511.1577).

2.15. [Ga(dedpa-propyl$_{pyr}$-NH$_2$-(N,N′-propyl-2-NI)][NO$_3$], [Ga(10)][NO$_3$]

The gallium complex was prepared as above for [Ga(**8**)][NO_3] using **10** and was isolated as a white solid. ^{1}H NMR (400 MHz, D_2O) δ 8.33 (s, 2H), 8.02 (s, 2H), 7.38 (s, 2H), 7.19 (s, 2H), 4.65 (d, $J = 17.1$ Hz, 2H), 4.47 (t, $J = 6.0$ Hz, 4H), 4.44 (d, $J = 9.7$ Hz, 2H), 3.25 (d, $J = 11.4$ Hz, 2H), 3.17 (dd, $J = 11.2$, 4.0 Hz, 8H), 2.86 (d, $J = 11.1$ Hz, 2H), 2.83 (d, $J = 9.9$ Hz, 2H), 2.49–2.38 (m, 2H), 2.38–2.23 (m, 4H), 2.21 (dt, $J = 15.8$, 7.9 Hz, 4H). ^{13}C NMR (101 MHz, D_2O) δ 163.3, 161.8, 148.8, 141.3, 126.8, 126.7, 126.0, 122.9, 116.3, 113.4, 54.4, 45.3, 37.3, 30.8, 25.3, 21.4. HR–ESI–MS m/z for $C_{34}H_{44}^{69}GaN_{12}O_8$ (M^+) calcd. (found) 817.2661 (817.2659) (−0.2 PPM).

2.16. [Ga(dedpa-propyl$_{pyr}$-FITC)][NO$_3$], [Ga(11)][NO$_3$]

To a solution of [Ga(**8**)][NO_3] (7.2 mg, 0.013 mmol) in water (0.5 mL), a solution of FITC (11.0 mg, 0.028 mmol, 2.2 equiv) in DMF/water

Please cite this article as: C.F. Ramogida, et al., Novel "bi-modal" H2dedpa derivatives for radio- and fluorescence imaging, J. Inorg. Biochem. (2015), http://dx.doi.org/10.1016/j.jinorgbio.2015.11.021

(2:1, 0.3 mL) was added. To this murky yellow solution, triethylamine (7 μL, 4 equiv) was added at which time the solution turned clear and became bright orange in color. The reaction mixture was stirred at ambient temperature under darkness for 18 h. The solution volume was reduced by ~2/3 by evaporation with blowing air, then the crude mixture was purified by RP-HPLC (gradient: A: 0.1% TFA (trifluoroacetic acid) in water, B: CH_3CN; 5 to 100% B linear gradient over 25 min, 1 mL/min, t_R (product) = 18.0 min). Product fractions were pooled and lyophilized to yield the product as a bright yellow solid (10.7 mg, 63%). Purity was confirmed by HPLC re-injection of an aliquot of final collected product. HR–ESI–MS m/z for $C_{64}H_{52}^{69}GaN_8O_{14}S_2$ (M^+) calcd. (found) 1289.2300 (1289.2291) (−0.7 PPM).

2.17. [Ga(dedpa-propyl$_{pyr}$-FITC-(N,N′-propyl-2-NI)][NO$_3$], [Ga(12)][NO$_3$]

The final product was prepared as above for [Ga(**11**)][NO_3] using **12** and was isolated as a bright yellow solid (5.2 mg, 45%, t_R (product) = 18.5 min). Maldi-TOF MS (ES+) m/z = 1595.6 [M^+].

2.18. Attempted Ga(III) complexation of derivatives 11 and 12

To a solution of **11** or **12** (0.02 mmol) in water/methanol (2:1, 0.5 mL), a solution of $Ga(NO_3)_3 \cdot 6H_2O$ (0.022 mmol, 1.1 equiv) in water (0.2 mL) was added. The pH of this solution was adjusted to 5 using aq. NaOH (0.1 M), and subsequently stirred at 60 °C for 40 min. The reaction progress was followed by ES–MS by presence of the $[M(L)]^+$ peak. No complexation was evident after 40 min, and the reaction was subsequently stirred at 90 °C overnight. Again, no complexation was evident.

2.19. 3D tumor spheroids cell culture and compound dosing

DLD-1 human colon carcinoma cells were maintained in Advanced DMEM (Invitrogen) and supplemented with 2% FBS and 2 mM glutamine in a humidified incubator at 37 °C and 5% CO_2. Spheroid culture procedures followed those of a previously reported protocol. [30,31] Spheroids were formed by plating 100 μL of a 1.5×10^5 cell mL^{-1} single cell suspension of DLD-1 cells onto agarose (0.75%) coated 96 well plates and they were allowed to aggregate for 5 to 7 days which resulted in the formation of one spheroid per well. Stock solutions (S_o) of $[Ga(\mathbf{11})]^+$, $[Ga(\mathbf{12})]^+$, **11**, and **12**, and FITC were made up in media with 6% DMSO to an original concentration of approx. 0.6 mM. Aliquots of each stock solution (S_o) were used to make working solutions (S_{100}, S_{20}, S_5) of 100, 20, and 5 μM for each compound. These were dosed in triplicate for each independent compound, concentration, and time point. At the time of dosing, 50 μL of medium from each well containing a spheroid was replaced with 50 μL of each working solution S_{100}, S_{20} or S_5 such that the final concentration of compound in the well was 50, 10, or 2.5 μM, respectively (final concentration of DMSO in each well did not exceed 1%). Dosed spheroids were then incubated at 37 °C for 1, 2, or 4 h. At the end of each incubation period, spheroids were transferred to 1.5 mL Eppendorf tubes and washed thrice with phosphate buffered saline (PBS, pH 7.4, 3 × 200 μL) to remove excess compound. Spheroids were then transferred to a 96-well imaging plate.

2.20. Confocal microscopy imaging

Confocal images were taken on an Olympus Fluoview FV1000-inverted laser scanning confocal microscope located in the Life Sciences Centre at the University of British Columbia. The microscope was equipped with an Olympus UPLAPO 10×/0.40 air objective lens, UPLAPO 40×/1.00 oil objective lens and PLAPO 60×/1.40 water objective lens. A scan rate of 4.0 μs $pixel^{-1}$ with Kalman averaging was used. The argon 488 nm laser had the following excitation and emission ranges: Ex 488 nm: Em 500–550 nm. Images were processed with ImageJ software, and displayed images are all at a depth (measurement along z-axis) of 144.3 μm.

3. Results and discussion

3.1. Synthesis and characterization of pro-ligands and metal complexes

In an attempt to fully harness the potential of H_2dedpa for radiopharmaceutical elaboration, much effort has been made towards developing new and facile synthetic routes towards preparation of bifunctionalized analogs of the native unfunctionalized scaffold. These bifunctional chelating ligands (BFCs) should possess reactive groups for bioconjugation to targeting vectors. Herein, a novel BFC based on the strong Ga(III) chelate H_2dedpa has been developed where bis-functionalization has been introduced through the 4-position of each pyridyl group (H_2dedpa-propyl$_{pyr}$-NH_2, **8**).

Preparation of the novel BFC (**8**), began with the conversion of chelidamic acid to methyl 4-bromo-6-(bromomethyl)picolinate (**3**) in three steps (55% overall yield, Scheme 1). This bromo-picolinate was used in *N,N′*-alkylation of 2-nitrobenzenesulfonamide (nosyl) protected ethylenediamine [16] to yield **4** in high yield (89%, Scheme 2). The di-bromo substituents on the nosyl-protected Me_2dedpa precursor **4** were cross-coupled to *tert*-butyl-prop-2-yn-1-ylcarbamate (Boc-N propargylamine) using Sonogashira methodology to yield **5** (78% yield). In order to prevent unwanted nucleophilic addition of thiophenol to the alkynes, the alkyne bonds were reduced under mild conditions (10% Pd on activated carbon, H_2) to produce the analogous alkane product **6** (84% yield) before nosyl-deprotection was performed. The alkyne reduction reaction was monitored closely and quenched before reduction of the nitro moieties off the nosyl groups began. Both nosyl groups were removed through the addition of thiophenol under basic conditions to yield protected pro-ligand **7** (63% yield). Methyl ester and N-Boc deprotections were performed in one-pot to yield the novel bifunctional H_2dedpa analog H_2dedpa-propyl$_{pyr}$-NH_2 (**8**) (26% overall yield in 5 steps). Compound **8** contains two primary amines as reactive sites for further conjugation to biomolecules.

The protected pro-ligand **7** was also further functionalized off the secondary amines with 1-(3-bromopropyl)-2-nitroimidazole, followed by complete deprotection to give **10**; this scaffold now contains 2-nitroimidazoles, which are common trapping moieties in hypoxic tissue, as well as two primary amines situated off the 4-position of the pyridyl rings which can be used in further bioconjugation reactions.

As a proof-of-principle, fluorescein isothiocyanate (FITC) was conjugated to the reactive primary amines of BFCs **8** and **10** (Scheme 3)

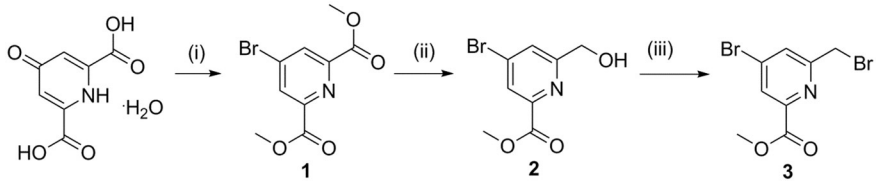

Scheme 1. Synthesis of methyl 4-bromo-6-(bromomethyl)picolinate (**3**). Reagents and conditions: (i) a. PBr_5, N_2, 90 °C, 2 h; b. $CHCl_3$, methanol, 0 °C (ii) methanol/CH_2Cl_2, $NaBH_4$, 0 °C, 1.5 h (iii) PBr_3, $CHCl_3$, 0 °C – RT, 3.5 h.

Please cite this article as: C.F. Ramogida, et al., Novel "bi-modal" H2dedpa derivatives for radio- and fluorescence imaging, J. Inorg. Biochem. (2015), http://dx.doi.org/10.1016/j.jinorgbio.2015.11.021

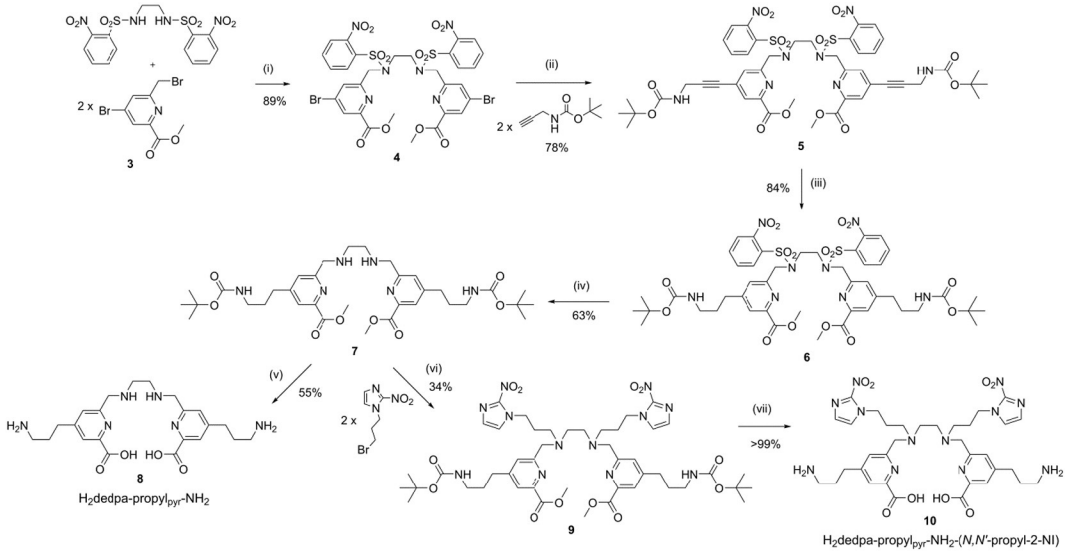

Scheme 2. Synthesis of novel pyridyl-functionalized H_2dedpa BFCs H_2dedpa-propyl$_{pyr}$-NH_2 (**8**) and H_2dedpa-propyl$_{pyr}$-NH_2-(*N,N′*-propyl-2-NI) (**10**). Reagents and conditions: (i) DMF, Na_2CO_3, RT, 3 d; (ii) THF, Et_3N, $Pd(PPh_3)_2Cl$, CuI, N_2, 60 °C, 18 h; (iii) EtOAc, Pd/C, H_2, RT, 2 × 24 h; (iv) THF, thiophenol, K_2CO_3, RT, 4 d; (v) THF/water (3:1), LiOH, RT, 1 h, then 4 M HCl/dioxane/THF (3:2:1), RT, 18 h; (vi) CH_3CN, K_2CO_3, 55 °C, 4 d; (vii) same as (v).

through thiourea bond formation, to generate "bi-modal" imaging probes. FITC is a commercially available fluorophore ($\lambda_{ex}/\lambda_{em}$ = 490/525 nm) used commonly as a dye in fluorescence microscopy and cell biology because of its high absorptivity, excellent fluorescence quantum yield, and good water solubility. The pro-ligand **11** contains both the promising backbone H_2dedpa (N_4O_2) for chelation to radiometals $^{67/68}$Ga, as well as the fluorophore FITC for optical imaging. Similarly, **12** also contains both the chelating backbone (N_4O_2) and fluorophore, but also 2-nitroimidazole moieties which will act as hypoxia targeting/trapping vectors.

Complexation of each pro-ligand (**11** and **12**) with non-radioactive gallium was also attempted, but was unsuccessful. No evidence of metal complexation was observed by ESI–MS, NMR, or HPLC analysis, even when the reaction mixture was heated to reflux overnight. Instead, the 'fluorophore-free' precursors **8** and **10** were allowed to complex with Ga(III) under the mild conditions previously used for unfunctionalized H_2dedpa (Scheme 3). The Ga-precursors [Ga(**8**)]$^+$ and [Ga(**10**)]$^+$ were isolated and fully characterized by HR–ESI–MS, and NMR spectroscopy. Diagnostic diastereotopic splitting of hydrogens in the ethylenediamine bridge was tracked by NMR spectroscopy. These two Ga-complexes were then successfully conjugated to FITC under basic conditions, and purified by RP-HPLC to give [Ga(**11**)]$^+$ and [Ga(**12**)]$^+$ as bright yellow solids. Again, the diastereotopic splitting of hydrogens in the metal complexes was identified in the ^{1}H NMR spectrum (Fig. 2). The absorption and emission spectra of [Ga(dedpa-propyl$_{pyr}$-FITC)]$^+$, [Ga(**11**)]$^+$, revealed excitation and emission peaks at 492 and 527 nm respectively (Fig. 3), which are typical for wavelengths of the FITC dye.

3.2. ^{67}Ga radiolabeling studies

The γ-emitter ^{67}Ga ($t_{1/2}$ = 3.26 d) was used in initial radiolabeling studies of the novel bi-modal ligands **11** and **12** to determine their abilities to complex gallium isotopes. Because of its longer half-life, ^{67}Ga was used as a model for ^{68}Ga in the radiolabeling experiments performed herein. Unfortunately, neither fluorescent ligand (**11** or **12**) displayed any ^{67}Ga labeling (radiochemical yield ~0%) under 10 min and room temperature reaction conditions. Extended reaction times and elevated temperatures (1 h, 85 °C) did not result in an increase in radiolabeling yield. Although disappointing, this result was not surprising since direct complexation of the ligands **11** and **12** with non-radioactive gallium was also futile (vide supra). It is hypothesized that the added structural 'bulk' introduced by two fluorescein molecules (MW = 389.3 Da each) dangling from the 4-position of each pyridyl ring impedes the movement/reorganization of donor atoms of the metal binding sphere of the linear H_2dedpa chelate, thus obstructing metal complexation. Moreover, fluorescein contains many functional groups that can potentially interfere with chelation of gallium. For example, the highly acidic phenolic acid moieties as well as the acid–base tautomeric equilibria of lactone to carboxylate are potential functionalities that can compete for metal chelation. Given this possibility,

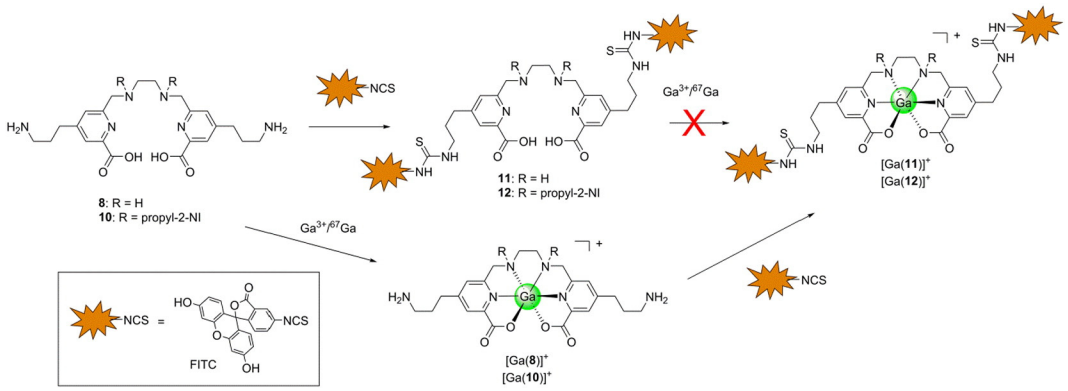

Scheme 3. Synthesis of bi-modal H_2dedpa derivatives H_2dedpa-propyl$_{pyr}$-FITC (**11**) and H_2dedpa-propyl$_{pyr}$-FITC-(*N,N′*-propyl-2-NI) (**12**) and corresponding Ga-complexes.

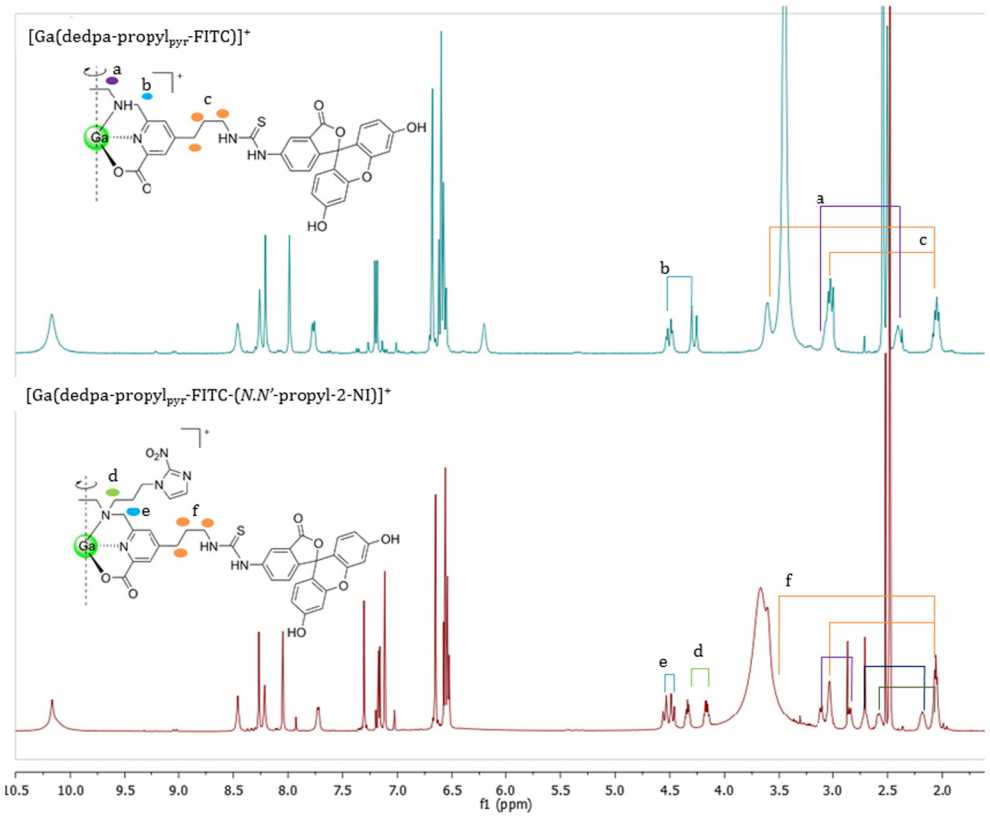

Fig. 2. ^{1}H NMR spectra of (top) [Ga(dedpa-propyl$_{pyr}$-FITC)]$^+$ ([Ga(**11**)]$^+$) and (bottom) [Ga(dedpa-propyl$_{pyr}$-FITC-(*N,N'*-propyl-2-NI)]$^+$ ([Ga(**12**)]$^+$) in DMSO-d$_6$ (400 MHz, 25 °C) highlighting diastereotopic splitting due to gallium complexation.

the lack of metal chelation for fluorescent dedpa ligands **11** and **12** may be from a combination of steric and functional group interference.

Consequently, precursors without the fluorescent probe (**8** and **10**) were labeled with ^{67}Ga as a model. Both displayed quantitative ^{67}Ga labeling (RCY > 99%) under reaction conditions commensurate with unfunctionalized H$_2$dedpa [17] and its recently reported 2-NI derivatives [23] (10 min at room temperature, 10^{-4} to 10^{-5} M ligand).

3.3. Human apo-transferrin stability studies

^{67}Ga-labeled precursors **8** and **10** were tested in a human *apo*-transferrin stability assay, and were used as a model to assess the kinetic inertness of the bi-modal H$_2$dedpa derivatives. Radiolabeling of the final 'bi-modal' probed **11** and **12** was unsuccessful, and therefore could not be tested in the *apo*-transferrin challenge assay. The iron transport protein in humans, transferrin, possesses a strong binding affinity for Fe(III) and other similar metal ions, especially Ga(III). Consequently, it is imperative that any chelate-bound $^{67/68}Ga^{3+}$ be sufficiently stable (both thermodynamically stable and kinetically inert) to prevent transchelation of the radiometal to the endogenous protein in vivo. The unaltered H$_2$dedpa ligand previously demonstrated exceptional stability in a human *apo*-transferrin stability assay remaining >99% intact after 2 h, [17] this result is compared to ligand **8** from this work where propyl linkers in the 4-position of the pyridyl rings have been added to introduce bifunctionality of the native H$_2$dedpa scaffold (Table 2). [^{67}Ga(**8**)]$^+$ exhibited slightly reduced stability after 2 h compared to [^{67}Ga(dedpa)]$^+$ (93 versus >99% intact). A similar trend was seen when comparing analogs which include 2-NI moieties (**10** and H$_2$dedpa-*N,N'*-propyl-2-NI): [^{67}Ga(**10**)]$^+$ was approximately 27% less stable than the corresponding complex in which there is no pyridyl functionalization ([^{67}Ga(dedpa-*N,N'*-propyl-2-NI)]$^+$). These results suggest that functionalization of H$_2$dedpa at the 4-position of the pyridyl rings leads to complexes of (somewhat) reduced kinetic inertness. The propyl linker serves as a weak electron donor and introduces some degree of steric 'bulk' around the metal binding pocket of the ligand. These steric and electronic effects imposed by the addition of the alkyl linker seemed to have translated to ligands of reduced stability compared to their unfunctionalized analogs. Furthermore, it is also possible that intramolecular interaction of the chelated ^{67}Ga(III) with nucleophilic primary amine moieties of derivatives **8** and **10** may affect the stability of the resultant metal complex. Further stability studies with Ga-complexes in which the amines have been acylated with placeholders (e.g. benzyl groups) prior to complexation are planned in the future to discern the stability of these derivatives compared to those which possess free primary amines (e.g. derivatives **8** and **10**).

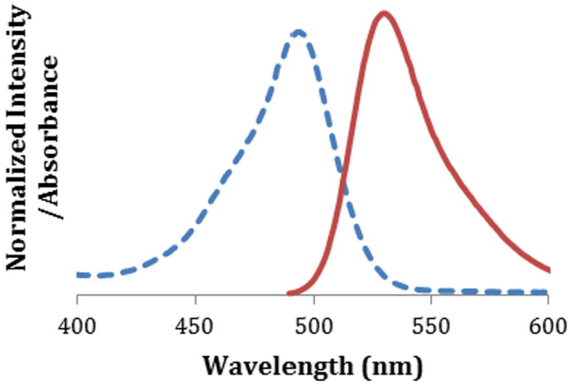

Fig. 3. Excitation (blue dashed) and emission (red solid, $\lambda_{ex} = 490$ nm) spectra of [Ga(**11**)]$^+$, [Ga(dedpa-propyl$_{pyr}$-FITC)]$^+$, in PBS (pH 7.4). (For interpretation of the references to color in this figure legend, the reader is referred to the web version of this article.)

Table 2
apo-Transferrin stability challenge assay (37 °C, 2 h) of ^{67}Ga-labeled pyridyl-functionalized dedpa^{2-} ligands **8** and **10**, and non-functionalized dedpa^{2-} standards for comparison, with stability shown as the percentage of intact ^{67}Ga complex.

Complex	15 min (%)	1 h (%)	2 h (%)
$[^{67}Ga(\mathbf{8})]^+$	99.0 ± 0.9	92.3 ± 2.3	92.7 ± 2.2
$[^{67}Ga(\mathbf{10})]^+$	87.8 ± 3.1	82.3 ± 2.4	72.4 ± 2.0
$[^{67}Ga(dedpa)]^+$ [17]	>99	>99	>99
$[^{67}Ga(dedpa\text{-}N,N\text{-}propyl\text{-}2\text{-}NI)]^+$ [23]	97.6 ± 1.2	97.2 ± 0.9	>99

3.4. In vitro 3D spheroid imaging

The uptake of the novel fluorescent Ga-dedpa probes was tested in a multicellular spheroid model and visualized using confocal microscopy. Spheroids are multicellular 3-dimensional structures of cancerous cells that act as in vitro tumor models [32]. Multicellular spheroids can effectively simulate the features of solid tumors in vivo such as tumor micro-environment, cell–cell interactions, and the extracellular matrix; accordingly, they have found great utility for screening of potential drug candidates [30,33–35]. It has been shown that cells on the periphery of the spheroid actively proliferate and act as well-oxygenated healthy (normoxic) cells, while diffusion of oxygen near the centre of the spheroid is limited and hence cells at the centre are hypoxic [30]. Thus 3D spheroids are a good model for visualizing the distribution and targeting ability of fluorescent drugs in hypoxic conditions.

Spheroids were treated with both Ga-complexes, $[Ga(\mathbf{11})]^+$ and $[Ga(\mathbf{12})]^+$ at concentrations of 50, 10, and 2.5 μM and incubated for 1, 2, or 4 h to track the course of fluorescence uptake over time. The only difference between these two fluorescent probes is the addition of two 2-NI moieties on $[Ga(\mathbf{12})]^+$. It was hypothesized that the addition of hypoxia trapping functionalities onto $[Ga(\mathbf{12})]^+$ would result in specific uptake of the fluorescent probe in the hypoxic core of the spheroid, whilst $[Ga(\mathbf{11})]^+$ would display no such preference in cell uptake. Pro-ligands **11** and **12**, and FITC were also treated as controls. After removal of excess fluorescent probe and washing of spheroids with phosphate buffered saline, each was imaged using fluorescence confocal microscopy. Spheroids used for imaging were grown for either 5 or 7 days. As spheroids mature their cells pack more densely in the core resulting in reduced oxygen diffusion near the centre of the spheroid, hence older spheroids tend to be more hypoxic [32].

Spheroids (grown for 5 days) treated with $[Ga(dedpa\text{-}propyl_{pyr}\text{-}FITC\text{-}(N,N'\text{-}propyl\text{-}2\text{-}NI))]^+$ yielded confocal microscopy images with slight observable uptake of tracer, but no discernable elevated uptake of the 2-NI probe in the central hypoxic core of the spheroid over the course of 4 h (Fig. 4). Fluorescence images of 'negative control' $[Ga(dedpa\text{-}propyl_{pyr}\text{-}FITC)]^+$ exhibited some non-specific uptake evinced by even distribution of fluorescence throughout the spheroid over the course of 4 h. Due to the qualitative nature of the fluorescent images, it was impossible to discern real differences in probe uptake between $[Ga(\mathbf{11})]^+$ and $[Ga(\mathbf{12})]^+$ with 5 day old spheroids. Nonetheless, the results show that the novel fluorescent probes $[Ga(\mathbf{11})]^+$ and $[Ga(\mathbf{12})]^+$ were successfully imaged using fluorescence confocal microscopy in an in vitro 3D spheroid model.

Spheroids grown for 7 days were similarly treated with 10 μM of both $[Ga(dedpa\text{-}propyl_{pyr}\text{-}FITC\text{-}(N,N'\text{-}propyl\text{-}2\text{-}NI))]^+$ and $[Ga(dedpa\text{-}propyl_{pyr}\text{-}FITC)]^+$ for 2 h. It is evident that the 2-NI-containing probe ($[Ga(\mathbf{12})]^+$) exhibits elevated and concentrated localization near the central hypoxic core of the spheroid compared to the negative control $[Ga(\mathbf{11})]^+$ which displays only some residual non-specific uptake distributed evenly throughout the spheroid (Fig. 5). These results clearly demonstrate the ability of $[Ga(dedpa\text{-}propyl_{pyr}\text{-}FITC\text{-}(N,N'\text{-}propyl\text{-}2\text{-}NI))]^+$ to specifically localize at the hypoxic region within the spheroid model. The evident difference between probe uptake in 5 or 7 day old spheroids may suggest that younger spheroids (5 days old) are not sufficiently hypoxic to warrant 2-NI trapping.

4. Conclusions

Herein we report the preparation of a novel bifunctional analog of the promising Ga(III) chelate H_2dedpa using Sonogashira cross-coupling chemistry. This H_2dedpa bifunctional chelate (BFC) has been altered to encompass two propyl-NH_2 functionalities at the 4-position of each pyridyl ring ($H_2dedpa\text{-}propyl_{pyr}\text{-}NH_2$). The two primary amines in the H_2dedpa BFC **8** are sufficient for bioconjugation to targeting vectors bearing compatible reactive groups, such as an isothiocyanate. This new BFC was used in a conjugation reaction with the commercially

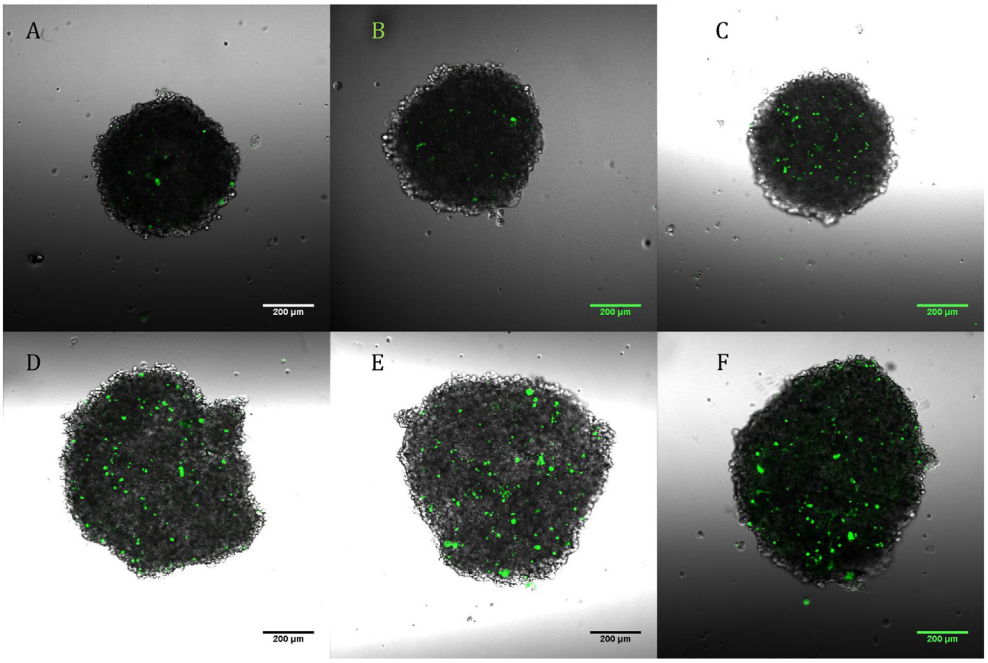

Fig. 4. Overlaid fluorescence (green) and optical (gray) images of 3D tumor spheroids (5 days old) treated with 10 μM $[Ga(dedpa\text{-}propyl_{pyr}\text{-}FITC\text{-}(N,N'\text{-}propyl\text{-}2\text{-}NI))]^+$, $[Ga(\mathbf{12})]^+$ (top row) or $[Ga(dedpa\text{-}propyl_{pyr}\text{-}FITC)]^+$, $[Ga(\mathbf{11})]^+$ (bottom row) incubated for (A,D) 1 h, (B,E) 2 h, or (C,F) 4 h.

Please cite this article as: C.F. Ramogida, et al., Novel "bi-modal" H2dedpa derivatives for radio- and fluorescence imaging, J. Inorg. Biochem. (2015), http://dx.doi.org/10.1016/j.jinorgbio.2015.11.021

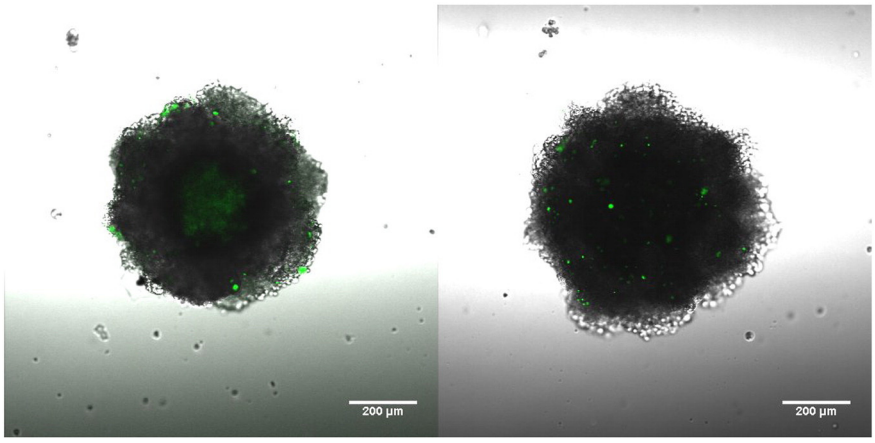

Fig. 5. Overlaid fluorescence (green) and optical (gray) images of 3D tumor spheroids (7 days old) dosed with (left) [Ga(dedpa-propyl$_{pyr}$-FITC-(*N*,*N*′-propyl-2-NI))]$^{+}$, [Ga(**12**)]$^{+}$, (right) negative control [Ga(dedpa-propyl$_{pyr}$-FITC)]$^{+}$, [Ga(**11**)]$^{+}$ (10 μM complex for 2 h). Highlighting elevated uptake of 2-NI fluorescent probe (left) in the central hypoxic core of the spheroid, compared to the negative control compound without 2-NI moieties (right).

available fluorophore FITC to generate a fluorescent H_2dedpa conjugate, as proof-of-principle. This "bi-modal" agent was evaluated for its potential as a combined ^{68}Ga PET and optical fluorescent imaging agent. A second H_2dedpa analog, which also contains two 2-NI moieties as a hypoxia marker in addition to the FITC fluorophore, was also successfully synthesized and characterized.

The addition of bulky fluorescein units suspended off each pyridyl ring of H_2dedpa precluded metal-complexation, and consequently resulted in unsuccessful ^{67}Ga radiolabeling. This result will ultimately limit the utility of these novel H_2dedpa fluorescent probes in future studies. Still, the 'fluorescent-free' precursors **8** and **10** were successfully radiolabelled with ^{67}Ga (>99% RCY, 10 min, RT), suggesting the new BFC, H_2dedpa-propyl$_{pyr}$-NH_2 (**8**), may be a promising candidate for conjugation with other lighter molecular weight targeting vectors. Human *apo*-transferrin stability assays of ^{67}Ga-labeled radiotracers **8** and **10** indicated that these BFCs form gallium complexes of good to moderate stability (93 and 72% intact after 2 h, respectively). Future studies to evaluate the mono-derivatization of the propylamine groups of the new bifunctional dedpa analog, H_2dedpa-propyl$_{pyr}$-NH_2 (**8**), are currently underway. Such derivatives can be used to add a protein-reactive group as well as a fluorophore onto the same chelate.

For the first time a novel fluorescent H_2dedpa derivative was synthesized, characterized, and successfully imaged using confocal fluorescence imaging in an in vitro 3D spheroid model. Fluorescence imaging using spheroids treated with a derivative in which the hypoxia marker 2-nitroimidazole was integrated resulted in specific localization of the fluorescent tracer in the central hypoxic core of the spheroid.

Abbreviations

BFC	bifunctional chelate(s)
CT	computed tomography
c(RGDyK)	cyclic(Arg–Gly–Asp–DTyr–Lys)
DOTA	1,4,7,10-tetraazacyclododecane-1,4,7,10-tetraacetic acid (N_4O_4)
FITC	fluorescein isothiocyanate
H_2dedpa	1,2-[[6-carboxy-pyridin-2-yl]-methylamine]ethane (N_4O_2)
MRI	magnetic resonance imaging
NI	nitroimidazole
NODAGA	1,4,7-triazacyclononane, 1-glutaric acid-4,7-acetic acid
NODASA	1,4,7-triazacyclononane-1-succinic acid-4,7-diacetic acid
Nosyl	2-nitrobenzenesulfonamide
NOTA	1,4,7-triazacyclononane-1,4,7-triacetic acid (N_3O_3)
PET	positron-emission tomography
pyr	pyridyl/pyridine
RCY	radiochemical yield
SPECT	single-photon emission computed tomography

Dedication

In memory of Professor Graeme Hanson and his contributions to Bioinorganic Chemistry and Electron Paramagnetic Resonance.

Acknowledgments

We acknowledge Nordion (Canada) and the Natural Sciences and Engineering Research Council (NSERC) of Canada for grant support (CR&D, Discovery) and NSERC CGS-M/CGS-D fellowships (to C.F.R.), the University of British Columbia for 4YF fellowships (to C.F.R.), and the UBC Centre for Blood Research for a summer student scholarship (J.D.R.). C.O. acknowledges the Canada Council for the Arts for a Killam Research Fellowship (2011–2013).

Appendix A. Supplementary data

Supplementary data to this article can be found online at http://dx.doi.org/10.1016/j.jinorgbio.2015.11.021.

References

[1] L.E. Jennings, N.J. Long, "Two is better than one"—probes for dual-modality molecular imaging, Chem. Commun. (Camb) (2009) 3511–3524, http://dx.doi.org/10.1039/b821903f.
[2] F.L. Thorp-Greenwood, M.P. Coogan, Multimodal radio- (PET/SPECT) and fluorescence imaging agents based on metallo-radioisotopes: current applications and prospects for development of new agents, Dalton Trans. 40 (2011) 6129–6143, http://dx.doi.org/10.1039/c0dt01398f.
[3] S. Keereweer, J.D.F. Kerrebijn, P.B.A.A. Van Driel, B. Xie, E.L. Kaijzel, T.J.A. Snoeks, et al., Optical image-guided surgery — where do we stand? Mol. Imaging Biol. 13 (2011) 199–207, http://dx.doi.org/10.1007/s11307-010-0373-2.
[4] D.K. Emerson, K.K. Limmer, D.J. Hall, S.-H. Han, W.C. Eckelman, C.J. Kane, et al., A receptor-targeted fluorescent radiopharmaceutical for multireporter sentinel lymph node imaging, Radiology 265 (2012) 186–193, http://dx.doi.org/10.1148/radiol.12120638.
[5] Y. Bernhard, P. Winckler, J.-M. Perrier-Cornet, R.A. Decréau, Harnessing medically relevant metals onto water-soluble subphthalocyanines: towards bimodal imaging and theranostics, Dalton Trans. 44 (2015) 3200–3208, http://dx.doi.org/10.1039/C4DT03536D.
[6] M.D. Bartholomä, A.S. Louie, J.F. Valliant, J. Zubieta, Technetium and gallium derived radiopharmaceuticals: comparing and contrasting the chemistry of two important radiometals for the molecular imaging era, Chem. Rev. 110 (2010) 2903–2920, http://dx.doi.org/10.1021/cr1000755.
[7] T.J. Wadas, E.H. Wong, G.R. Weisman, C.J. Anderson, Coordinating radiometals of copper, gallium, indium, yttrium, and zirconium for PET and SPECT imaging of disease, Chem. Rev. 110 (2010) 2858–2902, http://dx.doi.org/10.1021/cr900325h.

[8] C.F. Ramogida, C. Orvig, Tumour targeting with radiometals for diagnosis and therapy, Chem. Commun. (Camb.) 49 (2013) 4720–4739, http://dx.doi.org/10.1039/c3cc41554f.

[9] E.W. Price, C. Orvig, Matching chelators to radiometals for radiopharmaceuticals, Chem. Soc. Rev. 43 (2014) 260–290, http://dx.doi.org/10.1039/c3cs60304k.

[10] J.P. Andre, H.R. Maecke, M. Zehnder, L. Macko, K.G. Akyel, 1,4,7-Triazacyclononane-1-succinic acid-4,7-diacetic acid (NODASA): a new bifunctional chelator for radio gallium-labelling of biomolecules, Chem. Commun. (1998) 1301–1302, http://dx.doi.org/10.1039/A801294F.

[11] C.L. Ferreira, E. Lamsa, M. Woods, Y. Duan, P. Fernando, C. Bensimon, et al., Evaluation of bifunctional chelates for the development of gallium-based radiopharmaceuticals, Bioconjug. Chem. 21 (2010) 531–536, http://dx.doi.org/10.1021/bc900443a.

[12] I. Velikyan, G.J. Beyer, E. Bergström-Pettermann, P. Johansen, M. Bergström, B. Långström, The importance of high specific radioactivity in the performance of 68Ga-labeled peptide, Nucl. Med. Biol. 35 (2008) 529–536, http://dx.doi.org/10.1016/j.nucmedbio.2008.03.002.

[13] N. Viola-Villegas, A. Vortherms, R.P. Doyle, Targeting gallium to cancer cells through the folate receptor, Drug Target Insights 2008 (2008) 13–25.

[14] L.L. Chappell, B.E. Rogers, M.B. Khazaeli, M.S. Mayo, D.J. Buchsbaum, M.W. Brechbiel, Improved synthesis of the bifunctional chelating agent 1,4,7,10-tetraaza-N-(1-carboxy-3-(4-nitrophenyl)propyl)-N′,N″,N‴-tri s(acetic acid)cyclododecane (PA-DOTA), Bioorg. Med. Chem. 7 (1999) 2313–2320.

[15] E. Boros, C.L. Ferreira, D.T.T. Yapp, R.K. Gill, E.W. Price, M.J. Adam, et al., RGD conjugates of the H2dedpa scaffold: synthesis, labeling and imaging with 68Ga, Nucl. Med. Biol. 39 (2012) 785–794, http://dx.doi.org/10.1016/j.nucmedbio.2012.01.003.

[16] E. Price, B. Zeglis, J.F. Cawthray, C.F. Ramogida, N. Ramos, J.S. Lewis, et al., H4octapatrastuzumab: versatile acyclic chelate system for 111In and 177Lu imaging and therapy, J. Am. Chem. Soc. 135 (2013) 12707–12721, http://dx.doi.org/10.1021/ja4049493.

[17] E. Boros, C.L. Ferreira, J.F. Cawthray, E.W. Price, B.O. Patrick, D.W. Wester, et al., Acyclic chelate with ideal properties for 68Ga PET imaging agent elaboration, J. Am. Chem. Soc. 132 (2010) 15726–15733, http://dx.doi.org/10.1021/ja106399h.

[18] E. Boros, J.F. Cawthray, C.L. Ferreira, B.O. Patrick, M.J. Adam, C. Orvig, Evaluation of the H2)dedpa scaffold and its cRGDyK conjugates for labeling with 64Cu, Inorg. Chem. 51 (2012) 6279–6284, http://dx.doi.org/10.1021/ic300482x.

[19] A. Nunn, K. Linder, H.W. Strauss, Nitroimidazoles and imaging hypoxia, Eur. J. Nucl. Med. Mol. Imaging 22 (1995) 265–280, http://dx.doi.org/10.1007/BF01081524.

[20] W.R. Wilson, M.P. Hay, Targeting hypoxia in cancer therapy, Nat. Rev. Cancer 11 (2011) 393–410, http://dx.doi.org/10.1038/nrc3064.

[21] K.A. Krohn, J.M. Link, R.P. Mason, Molecular imaging of hypoxia, J. Nucl. Med. 49 (2008) 129S–148S, http://dx.doi.org/10.2967/jnumed.107.045914.

[22] M.R. Horsman, L.S. Mortensen, J.B. Petersen, M. Busk, J. Overgaard, Imaging hypoxia to improve radiotherapy outcome, Nat. Rev. Clin. Oncol. 9 (2012) 674–687, http://dx.doi.org/10.1038/nrclinonc.2012.171.

[23] C.F. Ramogida, J. Pan, C.L. Ferreira, B.O. Patrick, K. Rebullar, D.T.T. Yapp, et al., Nitroimidazole-containing H2dedpa and H2CHXdedpa derivatives as potential PET imaging agents of hypoxia with 68 Ga, Inorg. Chem. 54 (2015) 4953–4965, http://dx.doi.org/10.1021/acs.inorgchem.5b00554.

[24] L. Cui, Y. Zhong, W. Zhu, Y. Xu, Q. Du, X. Wang, et al., A new prodrug-derived ratiometric fluorescent probe for hypoxia: high selectivity of nitroreductase and imaging in tumor cell, Org. Lett. 13 (2011) 928–931, http://dx.doi.org/10.1021/ol102975t.

[25] H. Komatsu, H. Harada, K. Tanabe, M. Hiraoka, S. Nishimoto, Indolequinone–rhodol conjugate as a fluorescent probe for hypoxic cells: enzymatic activation and fluorescence properties, Med. Chem. Commun. 1 (2010) 50–53, http://dx.doi.org/10.1039/c0md00024h.

[26] E. Nakata, Y. Yukimachi, H. Kariyazono, S. Im, C. Abe, Y. Uto, et al., Design of a bioreductively-activated fluorescent pH probe for tumor hypoxia imaging, Bioorg. Med. Chem. 17 (2009) 6952–6958, http://dx.doi.org/10.1016/j.bmc.2009.08.037.

[27] K. Tanabe, N. Hirata, H. Harada, M. Hiraoka, S.I. Nishimoto, Emission under hypoxia: one-electron reduction and flourescence characteristics of an indolequinone-coumarin conjugate, Chembiochem 9 (2008) 426–432, http://dx.doi.org/10.1002/cbic.200700458.

[28] K. Okuda, Y. Okabe, T. Kadonosono, T. Ueno, B.G.M. Youssif, S. Kizaka-Kondoh, et al., 2-Nitroimidazole-tricarbocyanine conjugate as a near-infrared fluorescent probe for in vivo imaging of tumor hypoxia, Bioconjug. Chem. 23 (2012) 324–329, http://dx.doi.org/10.1021/bc2004704.

[29] K.E. Pryor, G.W. Shipps, D.A. Skyler, J. Rebek, The activated core approach to combinatorial chemistry: a selection of new core molecules, Tetrahedron 54 (1998) 4107–4124, http://dx.doi.org/10.1016/S0040-4020(98)00139-2.

[30] B.J. Kim, T.W. Hambley, N.S. Bryce, Visualising the hypoxia selectivity of cobalt(iii) prodrugs, Chem. Sci. 2 (2011) 2135–2142, http://dx.doi.org/10.1039/c1sc00337b.

[31] N.S. Bryce, J.Z. Zhang, R.M. Whan, N. Yamamoto, T.W. Hambley, Accumulation of an anthraquinone and its platinum complexes in cancer cell spheroids: the effect of charge on drug distribution in solid tumour models, Chem. Commun. (Camb.) (2009) 2673–2675, http://dx.doi.org/10.1039/b902415h.

[32] R. Sutherland, J. Carlsson, R. Durand, J. Yuhas, Spheroids in cancer research, Cancer Res. 41 (1981) 2980–2984http://cancerres.aacrjournals.org/content/41/7/2980.abstract.

[33] J.Z. Zhang, N.S. Bryce, R. Siegele, E.A. Carter, D. Paterson, M.D. de Jonge, et al., The use of spectroscopic imaging and mapping techniques in the characterisation and study of DLD-1 cell spheroid tumour models, Integr. Biol. 4 (2012) 1072–1080, http://dx.doi.org/10.1039/c2ib20121f.

[34] N. Yamamoto, A.K. Renfrew, B.J. Kim, N.S. Bryce, T.W. Hambley, Dual targeting of hypoxic and acidic tumor environments with a cobalt(III) chaperone complex, J. Med. Chem. 55 (2012) 11013–11021, http://dx.doi.org/10.1021/jm3014713.

[35] J.Z. Zhang, N.S. Bryce, A. Lanzirotti, C.K.J. Chen, D. Paterson, M.D. de Jonge, et al., Getting to the core of platinum drug bio-distributions: the penetration of anti-cancer platinum complexes into spheroid tumour models, Metallomics 4 (2012) 1209–1217, http://dx.doi.org/10.1039/c2mt20168b.

Please cite this article as: C.F. Ramogida, et al., Novel “bi-modal” H2dedpa derivatives for radio- and fluorescence imaging, J. Inorg. Biochem. (2015), http://dx.doi.org/10.1016/j.jinorgbio.2015.11.021